AGU100 ADVANCING EARTH AND SPACE SCIENCE

Paleoceanography and Paleoclimatology

RESEARCH ARTICLE
10.1029/2018PA003388

Key Points:
- This study discusses the lipid-based sea temperature reconstructions of the central Sea of Okhotsk
- The LDI reflects autumn sea surface temperature in core tops
- During glacial stages $U^{k'}_{37}$, TEX^{L}_{86}, and LDI reflect summer sea temperature

Supporting Information:
- Supporting Information S1

Correspondence to:
J. Lattaud and S. Schouten,
julie.lattaud@nioz.nl;
stefan.schouten1@uu.nl

Citation:
Lattaud, J., Lo, L., Huang, J.-J., Chou, Y.-M., Gorbarenko, S. A., Sinninghe Damsté, J. S., & Schouten, S. (2018). A comparison of late Quaternary organic proxy-based paleotemperature records of the central Sea of Okhotsk. *Paleoceanography and Paleoclimatology*, *33*. https://doi.org/10.1029/2018PA003388

Received 17 APR 2018
Accepted 15 JUN 2018
Accepted article online 23 JUN 2018

A Comparison of Late Quaternary Organic Proxy-Based Paleotemperature Records of the Central Sea of Okhotsk

Julie Lattaud[1], Li Lo[2,3], Jyh-Jaan Huang[4,5], Yu-Min Chou[6], Sergey A. Gorbarenko[7], Jaap S. Sinninghe Damsté[1,8], and Stefan Schouten[1,8]

[1]NIOZ Royal Netherlands Institute for Sea Research, Department of Marine Microbiology and Biogeochemistry, Utrecht University, Utrecht, Netherlands, [2]State Key Laboratory of Isotope Geochemistry, Guangzhou Institute of Geochemistry, Chinese Academy of Sciences, Guangzhou, China, [3]Department of Earth Sciences, University of Cambridge, Cambridge, UK, [4]Department of Geosciences, National Taiwan University, Taipei City, Taiwan, [5]Now at Institute of Geology, University of Innsbruck, Innsbruck, Austria, [6]Department of Ocean Sciences and Engineering, Southern University of Science and Technology, Shenzhe, China, [7]V.I. Il'ichev Pacific Oceanological Institute, Far East Branch Russian Academy of Science, Vladivostok, Russia, [8]Department of Earth Sciences, Faculty of Geosciences, Department of Earth Sciences, Utrecht University, Utrecht, Netherlands

Abstract The long-chain diol index (LDI) is a new organic sea surface temperature (SST) proxy based on the distribution of long-chain diols. It has been applied in several environments but not yet in subpolar regions. Here we tested the LDI on surface sediments and a sediment core from the Sea of Okhotsk, which is the southernmost seasonal sea ice-covered region in the Northern Hemisphere, and compared it with other organic temperature proxies, that is, $\mathbf{U^{k'}_{37}}$ and TEX^{L}_{86}. In the surface sediments, the LDI is correlated with autumn SST, similar to the $\mathbf{U^{k'}_{37}}$ but different from the TEX^{L}_{86} that correlates best with summer sea subsurface temperature. Remarkably, the obtained local LDI calibration was significantly different from the global core-top calibration. We used the local LDI calibration to reconstruct past SST changes in the central Sea of Okhotsk. The LDI-SST record shows low glacial (Marine Isotope Stage, MIS 2, 4, and 6) and high interglacial (MIS 1 and MIS 5) temperatures and follows the same pattern as the $\mathbf{U^{k'}_{37}}$-SST and a previously published TEX^{L}_{86} temperature record. Similar to the modern situation, the reconstructed temperatures during the interglacials likely reflect different seasons, that is, summer for the TEX^{L}_{86} and autumn for $\mathbf{U^{k'}_{37}}$ and LDI. During glacials, the reconstructed temperatures of all three proxies are similar to each other, likely reflecting summer temperatures as this was the only season free of sea ice. Our results suggest that the LDI is a suitable proxy to reconstruct subpolar seawater temperatures.

1. Introduction

Several organic proxies have been developed to reconstruct past sea surface temperatures (SST) in the geological record. The first organic SST proxy that was developed is the unsaturated ketone index ($\mathbf{U^{k'}_{37}}$), based on alkenone lipids synthesized by haptophyte algae (Brassell et al., 1986; Prahl & Wakeham, 1987). Culture studies showed that haptophyte algae adjust the degree of unsaturation of alkenones in response to growth temperature, with increased fractional abundances of the tri-unsaturated alkenone at lower temperatures. Subsequent work on surface sediments revealed that the $\mathbf{U^{k'}_{37}}$ index is strongly related to annual mean SST (Müller et al., 1998; Prahl et al., 1988). Another organic paleothermometer, the tetraether index (TEX_{86}), uses Thaumarchaeotal membrane lipids, that is, glyceryl dibiphytanyl glycerol tetraether lipids (GDGTs; Schouten et al., 2002). These Archaea synthesize GDGTs with an increasing number of cyclopentane moieties when seawater temperatures are higher and the TEX_{86} is strongly correlated with annual mean SST in global core-top data sets (Kim et al., 2010, 2015; Tierney & Tingley, 2015). However, both the $\mathbf{U^{k'}_{37}}$ and TEX_{86} proxies have their limitations. For example, the $\mathbf{U^{k'}_{37}}$ might be affected by nutrient availability, lateral transport, or oxic degradation (e.g., Gong & Hollander, 1999; Hoefs et al., 1998; Kim et al., 2009; Prahl et al., 2003; Rontani et al., 2013; Sikes et al., 2005) and the TEX_{86} by subsurface production of GDGTs and input of terrestrial GDGTs (e.g., Ho et al., 2014; Huguet et al., 2007; Kim et al., 2015; Shintani et al., 2011; Weijers et al., 2006). Furthermore, studies comparing $\mathbf{U^{k'}_{37}}$ and TEX_{86} show that they can reflect temperatures of different seasons of production and not annual mean temperature (Huguet et al., 2006; Jonas et al., 2017; Lopes dos Santos et al., 2013; Smith et al., 2013).

Recently, a new SST proxy, the long-chain diol index (LDI), was developed based on the distribution of long-chain diols (LCDs; Rampen et al., 2012), that is, the ratio of the C_{30} 1,15-diol over the sum of C_{28} 1,13; C_{30} 1,13; and C_{30} 1,15-diols, with higher fractional abundances of 1,15-diol observed at higher temperatures. The LDI seems to be independent from salinity but is impacted by freshwater input (De Bar et al., 2016; Lattaud, Kim, et al., 2017) and oxic degradation (Rodrigo-Gámiz et al., 2016). Nevertheless, the reconstruction of past SST using the LDI has been successful in various marine environments, predominantly in temperate regions (Jonas et al., 2017; Naafs et al., 2012; Plancq et al., 2015; Rampen et al., 2012; Rodrigo-Gámiz et al., 2014; Smith et al., 2013). However, the LDI has, up to now, never been applied in subpolar regions. Rodrigo-Gámiz et al. (2015) tested the application of the LDI in the North Atlantic Ocean, around Iceland, but the large amount of 1,14-diols (>80% of all LCDs), derived from *Proboscia* diatoms (Rampen et al., 2007; Sinninghe Damsté et al., 2003) obscured the LDI dependence to SST since *Proboscia* diatoms also produce minor amounts of 1,13-diols (Rampen et al., 2007), biasing the LDI toward colder SST.

Here we tested the applicability of the LDI in the Sea of Okhotsk. We generated high-resolution records of LDI-derived and $\mathbf{U^{k'}_{37}}$-derived SST for the past 180 ka from the central Sea of Okhotsk and compared this to a previously generated TEX_{86}-derived SST record (Lo et al., 2018). Furthermore, we also determined whether in the present-day environment the LDI, $\mathbf{U^{k'}_{37}}$, and TEX_{86} are reflecting annual mean or seasonal temperatures by analyzing a set of surface sediments from the Sea of Okhotsk.

2. Setting

2.1. Study Site

The Sea of Okhotsk is part of the Western Pacific Ocean and represents both the lowest-latitude and largest region with seasonal sea ice in the world (Harada et al., 2014). It is the second largest marginal subpolar sea of the Pacific after the Bering Sea. At present, in the Sea of Okhotsk, sea ice forms in the northwestern coastal area in November. Its maximum elongation goes as far south as northern Hokkaido, Japan, in March and disappears by June (Shimada & Hasegawa, 2001). The Sea of Okhotsk has many characteristics of a polar ocean: severe winters with cold air and strong northern winds, mild but short summers, large seasonal variation of air and water temperatures, and a subarctic water column structure (Wakatsuchi & Martin, 1991). The modern SST ranges from 13 °C in summer to −1 °C in winter (Figure 1b). According to Harada et al. (2014), autumn SST, sea surface salinity, and sea ice extent all impact the intensity of downwelling in the Sea of Okhotsk and, subsequently, control the formation of the Sea of Okhotsk Intermediate Water, which is a key component of the North Pacific Intermediate Water (itself an important carbon reservoir; Tsunogai et al., 1992). The Amur River in the northwest releases freshwater into the Sea of Okhotsk but most of its detrital loading does not reach the central part of the Sea of Okhotsk because the material is transported further to the south by lateral currents present in the Sea of Okhotsk (Yasuda et al., 2014).

2.2. Previous Paleoceanographic Studies

Several paleoceanographic studies on the Sea of Okhotsk have been performed. For example, Gorbarenko (1996) Gorbarenko et al. (2014) reconstructed periods of rapid warming and cooling during the Holocene and late Pleistocene, synchronous with the Greenland climatic cycles (glacial and interglacial stages as well as Heinrich events). SST reconstructions have been performed for the Holocene and the last glacial-interglacial interval using the $\delta^{18}O$ of planktonic foraminifera (Gorbarenko, 1996), as well as the TEX_{86} (Harada et al., 2012; Lo et al., 2018; Seki et al., 2009, 2014) and $\mathbf{U^{k'}_{37}}$ (Harada et al., 2004, 2006, 2014; Seki et al., 2004) temperature proxies. The reconstructed temperatures range from 5–7 °C to 8–12 °C for the TEX_{86} and from 4–7 °C to 8–12 °C for the $\mathbf{U^{k'}_{37}}$ for the last glacial maximum and the Holocene, respectively. These studies indicate that the alkenone and GDGT records reflect temperatures of different seasons, with the TEX_{86}-derived temperatures representing summer subsurface temperature (Lo et al., 2018; Seki et al., 2009, 2014) and the $\mathbf{U^{k'}_{37}}$-derived temperatures representing autumn SST (Seki et al., 2007).

3. Material and Methods

3.1. Sampling and Age Model

Giant piston core MD01-2414 (53°11.77′N, 149°34.80′E; Figure 1) was collected during the IMAGES VII cruise from the central region of the Sea of Okhotsk (Deyugin basin) at a water depth of 1,123 m in

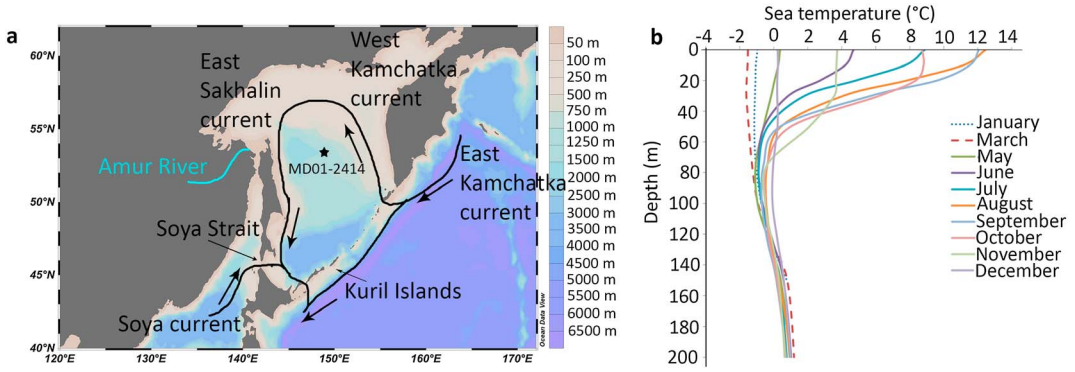

Figure 1. (a) Oceanographic setting of the Sea of Okhotsk and the location of core MD01 2414 and (b) monthly sea temperature (from NOAA; Locarnini et al., 2010) at this site.

2001 (Chou et al., 2011). This core has a length of 52.76 m but here we studied the upper 900 cm. This section was sampled every 10 cm, and the samples were stored frozen until freeze-dried. An age model for the core was established by Lo et al. (2018) based on the correlation of XRF data (log-ratios of (Ba/Ti)) with the global benthic foraminiferal $\delta^{18}O$ stack (LR04, Lisiecki & Raymo, 2005) and five accelerator mass spectrometry radiocarbon (AMS ^{14}C) dates of picked planktonic foraminifera (*Neogloboquadrina pachyderma*, *sinistral*).

Thirteen surface sediments were collected from the Sea of Okhotsk as described by Lo et al. (2018) (Figure 1).

3.2. Extraction and Separation of Lipids

The sediments were previously extracted by Lo et al. (2018). Briefly, sediment samples (1–10 g) were homogenized, freeze-dried, and extracted using dichloromethane (DCM): methanol (4: 1 *v*/v) using an accelerated solvent extractor. The extracts were separated into three fractions on a Pasteur pipette packed with activated Al_2O_3: an apolar fraction (hexane: DCM, 9:1 vol/vol), a ketone fraction (hexane: DCM, 1:1 vol/vol) containing alkenones, and a polar fraction containing the GDGTs and diols (DCM: MeOH, 1:1 vol/vol).

3.3. Alkenone Analysis and Determination of $U^{k'}_{37}$

Sedimentary alkenones were analyzed by dissolving the ketone fraction into 100 μl of hexane and using capillary gas chromatography (GC) with an Agilent 6890 N GC equipped with a silica column coated with CP Sil-5 (50 m × 320 μm; film thickness 0.12 μm), equipped with an on-column injector. The initial oven temperature of 70 °C increased with 20 °C/min to 200 °C and subsequently with 3 °C/min to 320 °C, at which it was held for 25 min. The carrier gas was helium at constant flow at 30 ml/min. Alkenones were detected with a flame ionization detector held at 330 °C.

The alkenone unsaturation index $\mathbf{U^{k'}_{37}}$ (Prahl & Wakeham, 1987) was calculated as follows:

$$U^{k'}_{37} = \frac{[C_{37:2}]}{[C_{37:2}] + [C_{37:3}]} \quad (1)$$

Several correlations between $\mathbf{U^{k'}_{37}}$ and water temperature have been reported (Müller et al., 1998; Prahl et al., 1988; Prahl & Wakeham, 1987; Sikes et al., 1997). The most often used global calibration of $\mathbf{U^{k'}_{37}}$ against annual mean SST is that of Müller et al. (1998):

$$SST = \frac{(U^{k'}_{37} - 0.044)}{0.033} \quad (2)$$

We applied the Bayspline calibration from Tierney and Tingley (2018) but no remarkable difference in absolute temperatures or trends with the calibration of Müller et al. (1998) was observed (maximum 0.7 °C).

3.4. LCD Analysis and Determination of LDI

LCDs were analyzed by silylation of an aliquot of the polar fraction with 10 μl BSTFA and 10 μl pyridine, heated for 30 min at 60 °C and adding 30 μl of ethyl acetate. The analysis of diols was performed using a gas chromatograph (Agilent 7990B GC), equipped with a capillary silica column coated with CP Sil 5 (25 m × 0.32 mm; film thickness 0.12 μm) and coupled with a mass spectrometer (Agilent 5977A MSD; GC-MS). Oven temperature during injection was 70 °C and increased thereafter to 130 °C at 20 °C/min and to 320 °C at 20 °C/min, at which it was maintained for 25 min. The flow of the carrier gas was held constant at 2 ml/min. The MS source was held at 250 °C and the MS quadrupole at 150 °C. The electron impact ionization energy of the source was 70 eV. The LCDs were identified and quantified via single-ion monitoring of the fragment ions *m/z* 299.3 (C_{28} 1,14-diol), 313.3 (C_{28} 1,13-diol; C_{30} 1,15-diol), 327.3 (C_{30} 1,14-diol), and 341.3 (C_{30} 1,13-diol; C_{32} 1,15-diol) following Versteegh et al. (1997) and Rampen et al. (2012). The abundance of the LCDs are expressed as fraction of the total LCDs quantified.

The long-chain diol index (LDI) is the ratio of C_{30} 1,15-diol over the sum of C_{30} + C_{28} 1,13-diols as defined by Rampen et al. (2012):

$$\boldsymbol{LDI} = \frac{[\boldsymbol{C_{30}1,15}]}{[\boldsymbol{C_{30}1,15}] + [\boldsymbol{C_{30}1,13}] + [\boldsymbol{C_{28}1,13}]} \tag{3}$$

The global calibration of LDI against annual mean SST (Rampen et al., 2012) is as follows:

$$\boldsymbol{SST} = \mathbf{0.033} \times \boldsymbol{LDI} + \mathbf{0.095} \tag{4}$$

3.5. GDGT Analysis and Determination of TEX_{86}

TEX_{86} (equation (5)); Schouten et al., 2002) values of the surface sediments and of the sediment core between 0 and 130 ka have been previously reported by Lo et al. (2018). Here we extended this record to 180 ka by analyzing 20 additional sediment samples for GDGTs following the methods described by Lo et al. (2018).

$$\boldsymbol{TEX_{86}} = \frac{\boldsymbol{GDGT-2} + \boldsymbol{GDGT-3} + \boldsymbol{Cren'}}{\boldsymbol{GDGT-1} + \boldsymbol{GDGT-2} + \boldsymbol{GDGT-3} + \boldsymbol{Cren'}} \tag{5}$$

A global calibration of the TEX^{L}_{86}, more suited for polar oceans, has been reported by Kim et al. (2010):

$$\boldsymbol{TEX^{L}_{86}} = \log\left(\frac{\boldsymbol{GDGT-2}}{\boldsymbol{GDGT-1} + \boldsymbol{GDGT-2} + \boldsymbol{GDGT-3}}\right) \tag{6}$$

$$\boldsymbol{TEX^{L}_{86}} - \boldsymbol{SST} = \mathbf{67.5} \times \boldsymbol{TEX^{L}_{86}} + \mathbf{46.9} \tag{7}$$

The Branched versus Isoprenoid Tetraether index (BIT) was calculated as described by Hopmans et al. (2004, 2016) with the inclusion of the 6-methyl branched GDGT from De Jonge et al. (2013) to infer if the GDGTs in the sediment core and surface sediments were affected by terrigenous input from the Amur River.

$$\boldsymbol{BIT} = \frac{\boldsymbol{Ia} + \boldsymbol{IIa} + \boldsymbol{IIIa} + \boldsymbol{IIa'} + \boldsymbol{IIIa'}}{\boldsymbol{Ia} + \boldsymbol{IIa} + \boldsymbol{IIIa} + \boldsymbol{IIa'} + \boldsymbol{IIIa'} + \boldsymbol{IV}} \tag{8}$$

4. Results and Discussion

4.1. Proxy Calibration

In all surface sediments alkenones, GDGTs and LCDs were detected. The $\mathbf{U^{k'}_{37}}$ ranges from 0.05 to 0.39, while the LDI varies from 0.02 to 0.44 (Figure 2). The TEX_{86} has previously been reported to vary from 0.18 to 0.34 (Lo et al., 2018). The BIT index is low in all surface sediments (0.02–0.12; Figure 5a) indicating relatively little input of terrestrial organic matter in these surface sediments (De Jonge et al., 2014; Hopmans et al., 2004; Weijers et al., 2006, 2009). The fractional abundance of the C_{32} 1,15-diol varies between 0.03 and 0.32 (Figure 5b), with higher fractional abundances close to the Soya Strait (0.20–0.32) compared to the northern and central part of the Sea of Okhotsk (0.03–0.10). This indicates input of riverine organic matter to the

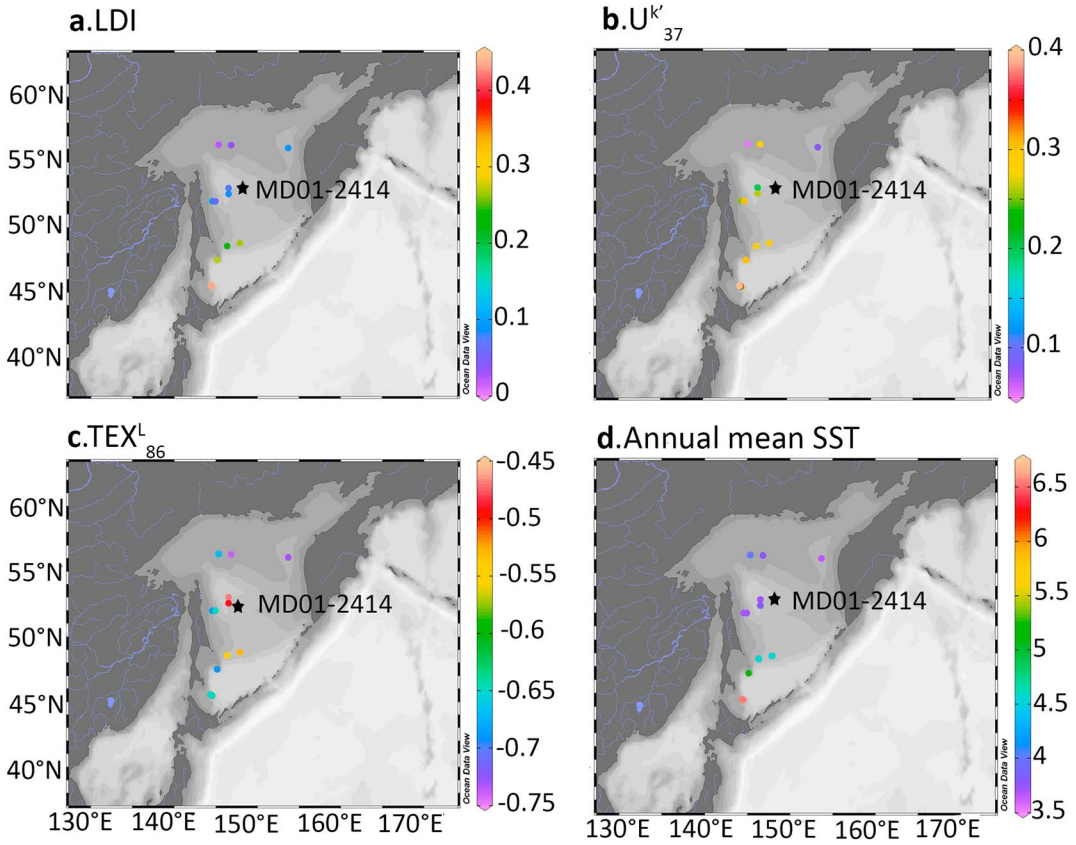

Figure 2. Geographical distribution of the values for (a) LDI, (b) $U^{k'}_{37}$, and (c) TEX^{L}_{86} of surface sediments and of (d) annual mean temperature (from NOAA; Locarnini et al., 2010).

southern part of the Sea of Okhotsk but shows that the northern and central parts of the Sea of Okhotsk are not influenced by riverine organic matter (cf. Lattaud, Kim, et al., 2017).

To determine if each proxies are reflecting seasonal or annual temperatures in modern days in the Sea of Okhotsk, we correlated the values of $\mathbf{U^{k'}_{37}}$, LDI, and the TEX^{L}_{86} from 13 surface sediments (Figure 2) with annual mean and seasonal SSTs (World Ocean Database, 2009, Locarnini et al., 2010).

The $\mathbf{U^{k'}_{37}}$ values are only weakly correlated with annual mean SST (Figure 3a; $r^2 = 0.24$, $p = 0.08$, $n = 13$) but the correlation obtained ($\mathbf{U^{k'}_{37}} = 0.039 \times SST + 0.0733$) is statistically identical (homogeneity of slope, $p = 0.98$) to the global calibration of Müller et al. (1998) (equation (2)**)**; Figure 3c). Indeed, the global calibration (equation (2)) has been shown to be suitable for estimating past temperatures in the subarctic region of the North Pacific, where *Emiliana huxleyi* is the main alkenone producer (Broerse et al., 2000) and has been applied earlier in the Sea of Okhotsk (Harada et al., 2004, 2006). However, *E. huxleyi* has been reported to bloom in autumn (late November to early December) in the Sea of Okhotsk (Broerse et al., 2000). Moreover, Seki et al. (2007) reported peak fluxes of alkenones in descending particles in the water column in autumn in the central Sea of Okhotsk and showed that $\mathbf{U^{k'}_{37}}$-derived temperature estimates from the collected sinking particles reflected autumn temperature of the shallow subsurface layer (20–30 m water depth). In the Sea of Okhotsk, autumn is a period with a strongly stratified water column and a warm and nutrient-depleted surface layer favoring the growth of *E. huxleyi* (Figure 1b). Indeed, we find a stronger correlation of the $\mathbf{U^{k'}_{37}}$ with late autumn SST (October–December, $\mathbf{U^{k'}_{37}} = 0.046 \times SST + 0.030$, $r^2 = 0.53$, $p < 0.005$, $n = 13$; Figure 3a) than with annual mean SST, suggesting that the $\mathbf{U^{k'}_{37}}$ reflects autumn temperatures rather than annual mean temperature in the Sea of Okhotsk. The significance of correlation with autumn temperatures decreases with deeper water temperature (e.g., 50 m, $r^2 = 0.29$, $p = 0.06$, $n = 13$; Figure 3a), suggesting that

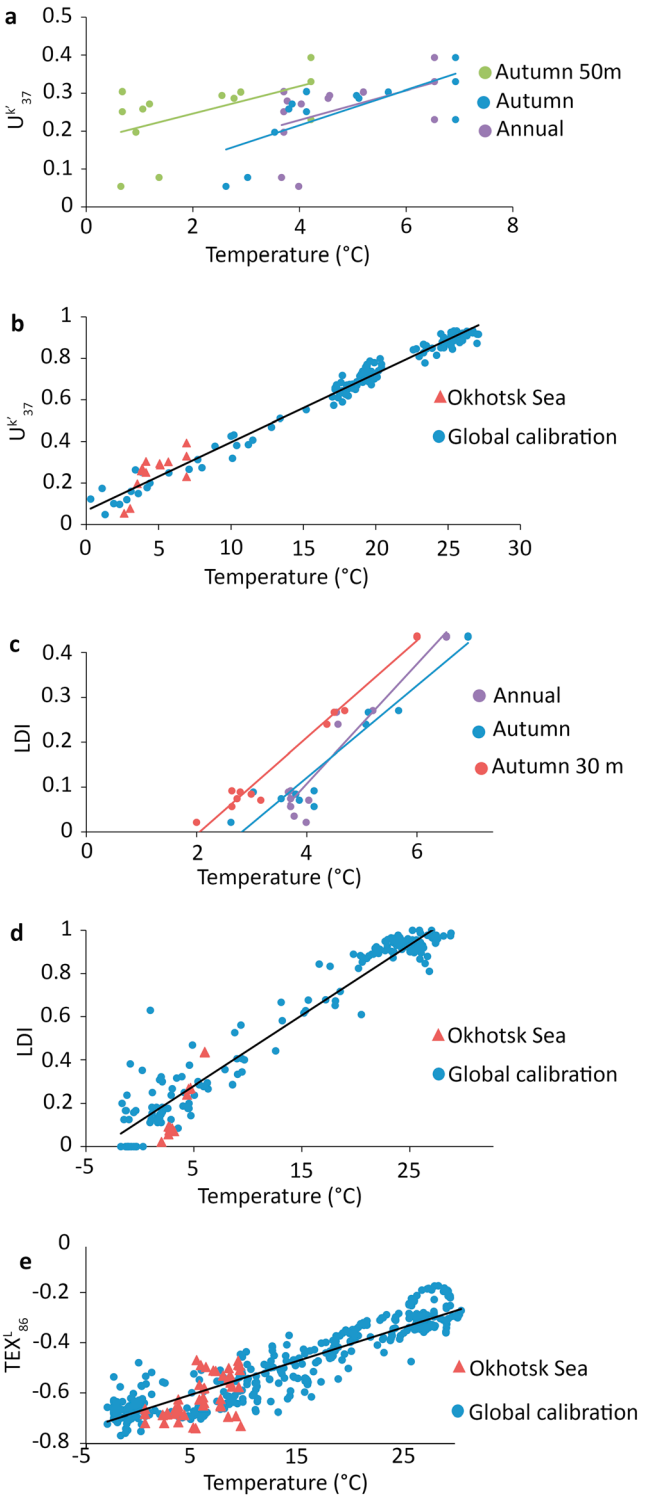

Figure 3. Correlation of observed sea temperature (from NOAA, Locarnini et al., 2010) with (a) $U^{k'}_{37}$, (b) $U^{k'}_{37}$ and the global data set of Müller et al. (1998), (c) LDI, (d) LDI and global data set of Rampen et al. (2012), and (e) TEX^{L}_{86} including the data of Seki et al. (2014) and the global data set of Kim et al. (2010).

$\mathbf{U^{k'}_{37}}$ reflects autumn SST in the Sea of Okhotsk. There is no significant (p = 0.95) difference between the global calibration of Müller et al. (1998) and the local autumn SST calibration. Furthermore, because the global calibration of Müller et al. (1998) is statistically more robust (n = 149 for the global calibration versus n = 13 for the local calibration), we use the global calibration for reconstructing autumn SST thereby also making our study comparable with other studies (Harada et al., 2004; Seki et al., 2007).

The LDI values of the surface sediments are strongly correlated with annual mean SST (Figure 3c; LDI = 0.133 × SST − 0.416, r^2 = 0.93, $p < 0.005$). This correlation is stronger than the correlation of $\mathbf{U^{k'}_{37}}$ with annual mean or autumn SST. Furthermore, in contrast to the $\mathbf{U^{k'}_{37}}$, this correlation differs significantly from the global core-top calibration of Rampen et al. (2012) (homogeneity of slopes, $p < 0.05$; Figure 3d). The LCD producers are likely phototrophic (eustigmatophyte) algae (Gelin et al., 1997; Méjanelle et al., 2003; Volkman et al., 1992, 1999), which proliferate in the photic zone. The relative proportion of 1,14-diols is low to moderate (13–43%) so we do not expect *Proboscia* diatoms to be a major source of the 1,13-diols. As the Sea of Okhotsk is partially frozen during the year (Shimada & Hasegawa, 2001), light penetration and nutrients will be limited during the winter and spring months, so it is likely that the LCDs are produced during a specific season rather than over the whole year and thus will likely reflect a seasonal rather than an annual mean signal. The LDI values are equally strongly correlated with autumn SST (Figure 3c; LDI = 0.103 × SST − 0.29, r^2 = 0.94, $p < 0.005$) as with annual mean. In contrast to the $\mathbf{U^{k'}_{37}}$, an even stronger correlation is observed with deeper water autumn temperatures, that is, at 20 m depth (Figure 3c; LDI = 0.108 × SWT − 0.222, r^2 = 0.98, $p < 0.005$, n = 13). However, the calibrations of the LDI for the autumn sea temperature at the surface and at 20 m are not statistically different (p = 0.95) and improvement of correlation coefficient is relatively small, and thus, it is not clear if the LDI is really reflecting SST or subsurface temperature. Based on the observation on phytoplankton dynamics in the Sea of Okhotsk, that is, diatoms are blooming in June as soon as the sea ice melts and the water column is rich in nutrients (Seki et al., 2007), while coccolithophorids are blooming in autumn when the water column is well stratified and nutrient-depleted (Seki et al., 2007), we assume that the LDI likely reflects autumn SST, when the competition with diatoms is less. Since the local calibration with autumn SST is significantly different from the global one, we used the former to reconstruct autumn SST (Figure 3d). This difference between the global and local calibration could be explained by the absence of Pacific surface sediments in the global calibration. Possibly, the diol producers in the Pacific Ocean might respond in their diol composition to temperature differently than those in the Atlantic Ocean.

We combined the reported TEX^{L}_{86} values of Lo et al. (2018) with those of Seki et al. (2014) to infer if the TEX^{L}_{86} is reflecting seasonal or annual sea temperature. The TEX^{L}_{86} values correlate weakly with annual mean SST (r^2 = 0.09, p = 0.03). Seki et al. (2007) suggested that the Thaumarchaeota, producing the GDGTs, may be blooming in late summer in the Sea of Okhotsk when enhanced ammonium concentration is observed between 20 and 45 m depth (in June 2000; Seki et al., 2014). Since Thaumarchaeota are ammonium oxidizers (De la Torre et al., 2008;

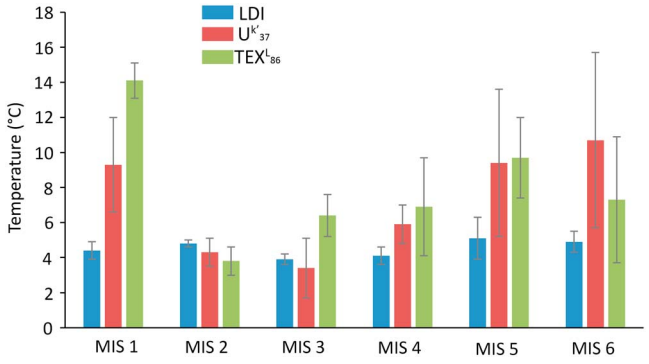

Figure 4. Average reconstructed temperature of the three paleothermometers and standard deviation during marine isotope stages (MIS 1: 0–14 ka, n = 16; MIS 2: 14–29 ka, n = 8; MIS 3: 28–57 ka, n = 8; MIS 4: 53–64 ka, n = 4; MIS 5: 64–130 ka, n = 26; and MIS 6: 130–180 ka, n = 20).

Wuchter et al., 2006), this time and depth may be the optimal time to proliferate. Indeed, the TEX^{L}_{86} correlates more significantly with summer sea subsurface temperatures at 20 m depth (SST = 0.018 × TEX^{L}_{86}-0.719, r^2 = 0.33, $p < 0.005$), while there is no significant correlation between TEX^{L}_{86} and summer SST (r^2 = 0.002, p = 0.4). There is a correlation between TEX^{L}_{86} and summer sea temperatures at 200 m depth (r^2 = 0.20, $p < 0.005$) but this correlation is weaker than with the summer sea temperature at 20 m depth. Alternatively, instead of TEX^{L}_{86}, we can use the original TEX_{86} definition (Schouten et al., 2002). However, correlation of the TEX_{86} of the surface sediments with the annual mean SST showed a weak correlation (r^2 = 0.11, p = 0.02). We also correlated TEX_{86} with summer sea temperature at 20 m and found a weak correlation (r^2 = 0.20, $p < 0.005$), weaker than with TEX^{L}_{86}. Therefore, it seems that TEX^{L}_{86} is best applicable for the Sea of Okhotsk. The regional calibration of TEX^{L}_{86} with summer sea temperatures at 20 m depth is not significantly different (homogeneity of slopes, p = 0.9) from the global core-top calibration with annual mean SST of Kim et al. (2010) (Figure 3c). Hence, we will thus use the global calibration, which is statistically more robust, but are probably reconstructing a summer sea subsurface temperatures (around 20 m depth) signal.

4.2. Temperature Variations Over the Last 180 ka as Recorded by Organic Proxies

Using the global calibrations for $\mathbf{U^{k'}_{37}}$ and TEX^{L}_{86} and the regional calibration of the LDI, we reconstructed temperatures over the last 180 ka in the Sea of Okhotsk. The LDI varies from 0.06 to 0.62, the $\mathbf{U^{k'}_{37}}$ varies from 0.07 to 0.72, and the TEX^{L}_{86} varies from −0.66 to −0.46 (TEX_{86} varies from 0.22 to 0.34). The three proxy records yield quite different absolute sea temperatures and trends (Figure 4). Nevertheless, LDI-derived and $\mathbf{U^{k'}_{37}}$-derived SST records show some significant correlation (r^2 = 0.13, p-value < 0.005), but with considerable scatter, and both are not correlated with TEX^{L}_{86}-derived temperatures (r^2 = 0.03 and 0.04, p-value > 0.05). This agrees with our findings for the surface sediments; that is, both LDI and $\mathbf{U^{k'}_{37}}$ are thought to reflect similar temperatures (autumn SST), while TEX^{L}_{86} reflects summer subsurface temperatures. However, a difference in seasonality cannot explain the lack of correlation between TEX^{L}_{86} and the other proxies, as we expect some correlation between seasonal temperatures. We also reconstructed temperatures using the BAYSPAR calibration (Tierney & Tingley, 2015) of TEX_{86} but this yielded mostly temperatures well below 0 (−7 to 3 °C), which seems unrealistic. LDI-derived SSTs also frequently differ from $\mathbf{U^{k'}_{37}}$-derived SSTs, especially during MIS 1, MIS 5, and MIS 6. These differences are often larger than the proxy calibration errors (2 and 1.5 °C, respectively).

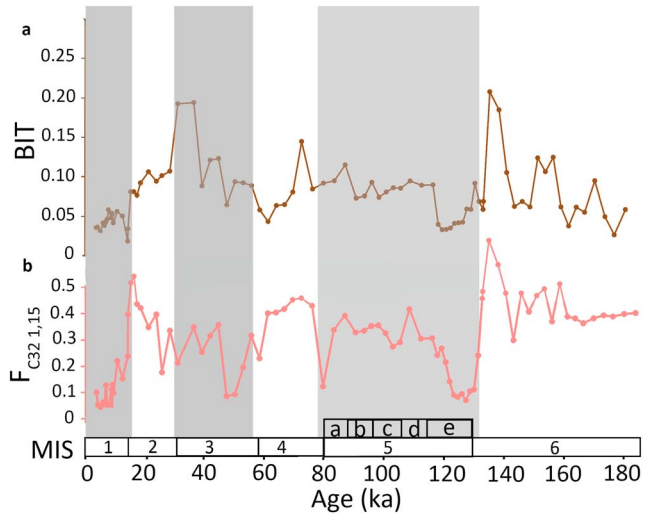

Figure 5. Terrigenous input proxies for core MD01–2414 (a) BIT index and (b) $F_{C32\ 1,15}$.

A general cause for the difference in the LDI temperature record and those of the $\mathbf{U^{k'}_{37}}$ could be input of LCDs from the Amur River as river input can affect the LDI (De Bar et al., 2016; Lattaud, Kim, et al., 2017; Lattaud, Dorhout, et al., 2017). The fractional abundance of C_{32} 1,15-diols (Figure 5b) in the sediment core is on average 0.33 ± 0.16, indicating some riverine input (cf. Lattaud, Kim, et al., 2017). It shows maxima at the start of Termination I and II, that is, at the end of MIS 2 (~0.5) and MIS 6 (~0.6), likely because of the low sea level stand at that time, maximizing the influence of the Amur River. We also observe a generally higher fractional abundance of C_{32} 1,15-diols (Figure 5b) during MIS 4. However, at times of a high fractional abundance of C_{32} 1,15-diols, no large variations in the LDI-SST record are observed, suggesting that river input of LCDs does not strongly affect the LDI (Figure 6a). The record of the BIT index (Figure 5a), a proxy for input of continental derived GDGTs (De Jonge et al., 2014; Hopmans et al., 2004; Weijers et al., 2006, 2009), also peaks at the end of MIS 6 but not at the end of MIS 2. Overall, it remains <0.2 (average 0.08 ± 0.04), suggesting that application of the TEX^{L}_{86} is not affected by terrigenous input from the Amur River. Below we discuss potential causes for

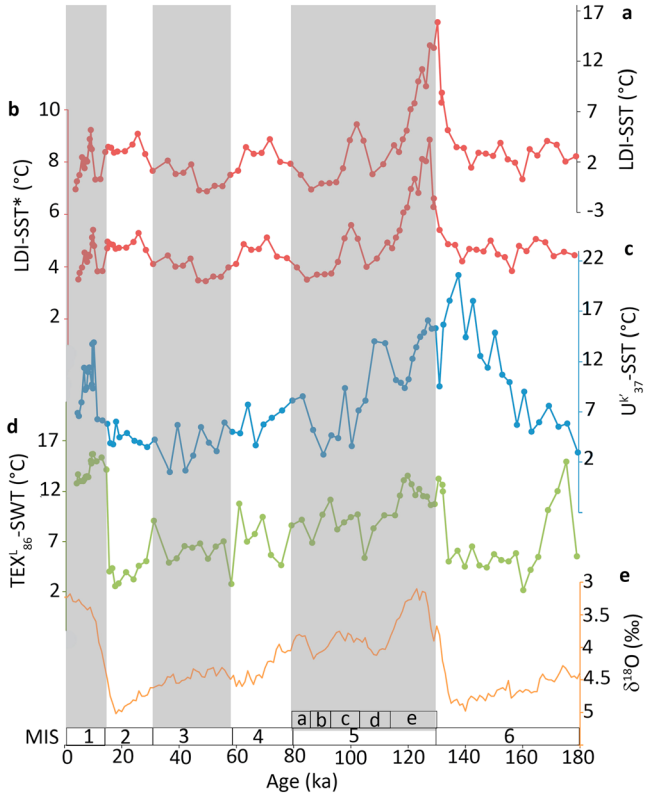

Figure 6. Reconstructed temperatures over the last 180 ka in comparison with the global LR04 stack. (a) LDI-SST (using the global calibration from Rampen et al., 2012), (b) LDI-SST* (using the local Okhotsk calibration), (c) $\mathbf{U^{k'}_{37}}$-derived SST and (d) TEX^{L}_{86}-derived temperatures (partly from Lo et al., 2018), and (e) $\delta^{18}O$ from the LR04 stack (Lisiecki & Raymo, 2005).

the difference between LDI reconstructed temperatures and those of other proxies in interglacial and glacial stages.

4.2.1. Sea Temperature Reconstructions During Interglacial Stages

During the early phase of MIS 5 the LDI shows a drop in temperature from 8.8 to 3.5 °C, while this drop for the $\mathbf{U^{k'}_{37}}$ record is from 16.0 to 2.8 °C (Figure 6a) and for the TEX^{L}_{86} record from 13.6 to 4.6 °C. MIS 5e (130–115 ka; Shackleton et al., 2003; Martrat et al., 2014) is the warmest period of the LDI temperature record (6.6 ± 1.3 °C), exceeding the modern day reconstructed LDI temperatures by 3 °C.

During the Holocene, both $\mathbf{U^{k'}_{37}}$ and LDI temperatures show a (sub) maximum at 9 ka, with $\mathbf{U^{k'}_{37}}$-SST reaching 9 °C, 4 °C (Figure 6b) higher than LDI-SST, while TEX^{L}_{86} reflects higher temperatures from 12 ka to 9 ka (15 °C). The warmest LDI and $\mathbf{U^{k'}_{37}}$ temperature at 9 ka falls during the Holocene Thermal Maximum (9–5 ka; Ritchie et al., 1983). This warm thermal event corresponded with the maximum northern extension of the warm Kuroshio current (Tsushima Current, Kuroshio culmination event; Harada et al., 2004) and, like during MIS 5e, incurred permanent ice-free condition in the entire Sea of Okhotsk (Lo et al., 2018; Nürnberg et al., 2011). This optimum is also observed in the $\mathbf{U^{k'}_{37}}$-SST records of Harada et al. (2004) and Martinez-Garcia et al. (2010) in the northwestern Pacific. Finally, there is a decrease of about 2 °C in LDI-derived temperatures in the late Holocene until modern days, reflecting the Late Holocene cooling observed by, for example, Martrat et al. (2014) in the North Atlantic region using $\mathbf{U^{k'}_{37}}$-derived SST reconstructions, and Russian terrestrial records (Salonen et al., 2011). This decrease is also observed in the Sea of Okhotsk and Northern Pacific records (via $\mathbf{U^{k'}_{37}}$ by Harada et al., 2014). Overall, the LDI-derived SSTs for the late Holocene are quite low; that is, we reconstructed the same temperatures for MIS 2 and the late Holocene. Potentially, these low temperatures could be explained by a shift in the season of production of the diols from summer (during MIS 2) toward autumn (during the Holocene). The $\mathbf{U^{k'}_{37}}$-SST also shows a lowering of temperatures during the late Holocene but remains higher than those during MIS 2.

Although LDI and $\mathbf{U^{k'}_{37}}$-SST records seem to match trend wise, in both interglacials MIS 1 and 5, there is a mismatch in absolute temperatures with $\mathbf{U^{k'}_{37}}$ being generally higher than those of the LDI, while our surface sediment study suggests both could reflect autumn SST. This could be due to the enhanced presence of diol-producing diatoms, that is, *Proboscia* (Rampen et al., 2011; Sinninghe Damsté et al., 2003) that produce 1,14-diols but also minor amounts of 1,13-diols that will biased the LDI temperatures toward colder values (Rodrigo-Gámiz et al., 2015). However, the amount of 1,14-diols is generally much lower than observed by Rodrigo-Gámiz et al. (2015) (up to 83% in Icelandic SPM against 33% for MIS 5 and for the Holocene in the Sea of Okhotsk), suggesting that this effect may be less. Alternatively, sea ice limits the penetration of light in the water column, so absence of sea ice (like during MIS 5e and 5c; Lo et al., 2018) extended the time period of light availability for primary producer. Thus, the blooming period of the haptophyte algae may have shifted or was extended to include warmer periods, such as summer and the blooming period of the diol producers could be extended to colder periods, such as spring. Indeed, $\mathbf{U^{k'}_{37}}$-SST temperatures are closer to TEX^{L}_{86}-temperatures, which reflect subsurface summer temperatures in the present-day Sea of Okhotsk, suggesting that they might have been blooming earlier in the season in between fall and summer.

4.2.2. Sea Temperature Reconstructions During Glacial Stages

In contrast to the interglacial stages, during the glacial stages (MIS 2, 4, and 6), the three temperature proxies yield similar temperatures (within proxy error, with the exception of MIS 6 for the $\mathbf{U^{k'}_{37}}$-SST; Figure 4) indicating that the proxies likely reflect the same season of production. This season is most likely summer as the Sea of Okhotsk is frozen during the remaining part of the year during glacial stages (Lo et al., 2018; Nürnberg et al.,

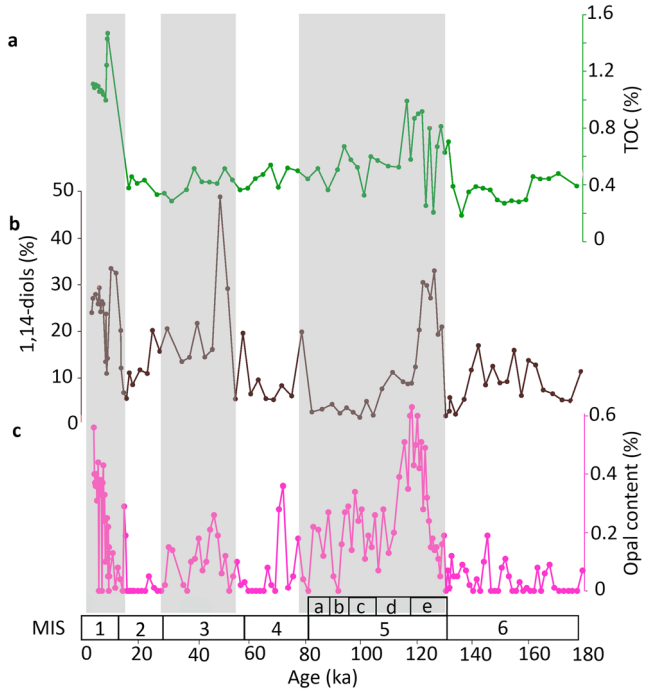

Figure 7. Productivity indicators in core MD01-2414 (a) TOC content, (b) fractional abundance of 1,14-diols, and (c) opal content (from Liu et al., 2006).

2011). The $U^{k'}_{37}$-derived SST record shows a continuous warming trend during MIS 6, in contrast to the other proxies (Figure 6b). During the late MIS 6, the $U^{k'}_{37}$-SSTs are unrealistically high; that is, the $U^{k'}_{37}$-derived SST was up to 16 °C higher than LDI-derived SST and TEX^{L}_{86} temperatures (Figures 6a and 6c). These temperatures are not plausible during a glacial stage that was much colder than modern day temperature (Lo et al., 2018; Nürnberg et al., 2011). These abnormally high $U^{k'}_{37}$-derived SSTs during late MIS 6 have also been observed by Martinez-Garcia et al. (2010) in sediments from the Northwestern Pacific and by Seki et al. (2009) in a core from the southern Sea of Okhotsk (51°N). These anomalous $U^{k'}_{37}$-derived SST values may be due to a contribution of allochtonous alkenones transported laterally (Mollenhauer et al., 2008), either from the warm Japan Sea via the Kuroshio current or from the relatively warmer Amur River delta further north. However, studies of sediment traps located 100 m above the seafloor in the present-day Sea of Okhotsk show no evidence for lateral transport of alkenones (Harada et al., 2006; Seki et al., 2007). These anomalous $U^{k'}_{37}$ values cooccur with an apparent input from the Amur River, as evidenced by the relatively higher BIT values (0.2; Figure 5a) and a high abundance of the C_{32} 1,15-diol between 140 and 134 ka (fractional abundance up to 0.7 of 1,13 and 1,15 LCDs at 134 ka; Figure 5b). This higher input is likely partly caused by the lower sea level during glacials, which will have moved the mouth of the Amur River closer to the core site. However, it is unclear how this enhanced river input would affect the $U^{k'}_{37}$ to anomalously high values, while the LDI and TEX^{L}_{86} do not seem to be affected. MIS 4 is not apparent as a strong glacial period in all three temperatures (Figure 4), as observed in the $\delta^{18}O$ of the LR04 stack (Figure 6d). The TEX^{L}_{86}-SST is particularly high (6.9 ± 2.8 °C), which could be due to enhanced terrestrial input as suggested by the relatively higher BIT index (0.14; Figure 5a) during that period.

MIS 2 (30–17 ka) is reflected as a cold stable period in the LDI temperature record (4.7 ± 0.3 °C; Figure 4) and temperatures are similar to those of the $U^{k'}_{37}$ and TEX^{L}_{86} records. During this period the Sea of Okhotsk was almost totally closed because of the shallow depth of the Soya Strait and Kuril Islands passes that were emerged during the low sea level stand of MIS 2 (Figure 1; Harada et al., 2004). This is similar to MIS 6, when sea ice also extended, and supported by relatively high IP_{25} concentrations, a proxy for seasonal ice cover (Belt et al., 2007; Knies et al., 2014), during MIS 2 (Lo et al., 2018). However, in contrast to MIS 6, the three temperature proxies all reveal similar temperatures, as would be expected if they are produced during the same season, that is, summer being the only ice-free season with substantial biological activity. Also, in MIS 2, there seems to be an enhanced input from the Amur River, as suggested by elevated values of the BIT index (0.14) and of $F_{C32\ 1,15}$ (0.43), although these are lower than observed during MIS 6. The termination (16–12 ka) of MIS 2 shows increasing TEX^{L}_{86} temperatures but a relatively constant LDI and $U^{k'}_{37}$-SST. This may be caused by a deepening of the production of alkenones and diols in the water column resulting in colder temperatures, as explained above, or by a shift from summer toward autumn SST (as found present day) for the LDI and $U^{k'}_{37}$, which would results in apparent relatively constant temperatures despite overall global warming.

4.3. Diatom Productivity in the Sea of Okhotsk

MIS 5e is characterized by a higher percentage of 1,14-diols (30% of all LCDs; Figure 7b), derived from *Proboscia* diatoms (Rampen et al., 2011; Sinninghe Damsté et al., 2003) and a high opal content (up to 0.63% at 129 ka; Figure 7c; from Liu et al., 2006), indicating increased diatom productivity (Leinen et al., 1986), and an increased TOC content (up to 0.81% at 129 ka; Figure 7a), suggesting higher primary productivity and, hence, more nutrient-rich water. This is supported by opal records from other cores from the Sea of Okhotsk (core PC3B, Iwasaki et al., 2012; and core GC09A, Khim et al., 2012; Bosin et al., 2015), with high opal content indicating high productivity during this time period. MIS 5e was characterized by open water

conditions in the central Sea of Okhotsk with no sea ice formation all year (Lo et al., 2018; Nürnberg et al., 2011). The absence of sea ice during MIS 5e allowed nutrients coming from the Amur River and the Pacific Ocean to reach the Sea of Okhotsk, thereby stimulating productivity.

Similar to MIS 5, there is evidence of an increase in diatomaceous production during the mid-Holocene with increase in biogenic opal content in the sediment (Figure 7c; Liu et al., 2006), paleontological indications of the remains of diatoms (Bosin et al., 2015), and increases in relative proportion of 1,14-diols (Figure 7b; up to 33%), as well as elevated TOC level (up to 1.5%), all suggesting increased (diatom) productivity. This agrees with the findings of Bosin et al. (2015), who showed that diatoms are the main primary producers presently in the Sea of Okhotsk (Sorokin & Sorokin, 1999) and that a phytoplankton transition occurred at the onset of the Holocene going from mainly haptophyte productivity toward a diatom productivity (Katsuki et al., 2010; Khim et al., 2012; Shiga & Koizumi, 2010).

5. Conclusions

Our study shows the applicability of the LDI as a proxy for SST in a polar region. The LDI-derived temperatures from surface sediments correlates well with autumn SST, similar to the $\mathbf{U^{k'}_{37}}$ but different than the TEX^{L}_{86}, which likely reflects summer subsurface temperature. Interestingly, the LDI-SST correlation is substantially different from the global core-top correlation, suggesting the importance of local calibrations. The LDI-derived SST record obtained from a sediment core in the central part of the Sea of Okhotsk shows temperature changes, generally in agreement with known global temperature changes during glacials and interglacials. The $\mathbf{U^{k'}_{37}}$, LDI and TEX^{L}_{86} temperature proxies yield similar temperatures during glacials, likely indicating the same season of production, that is, summer months as this was the only period without the presence of sea ice. In contrast, during interglacials when there is no sea ice, all three proxies yield different temperature representing different season and depth of production. Diatom productivity in the Sea of Okhotsk is reflected in the proportion of 1,14-diol and opal content of the sediment, showing increased productivity during terminations and during the Holocene.

Acknowledgments

J. L. Toney and J. Tierney are thanked for their constructive comments, which improved the manuscript. We thank Denise Dorhout, Jort Ossebaar, and Anchelique Mets for technical assistance. This research has been funded by the European Research Council (ERC) under the European Union's Seventh Framework Program (FP7/2007–2013) ERC grant agreement (339206) to S.S. The work was further supported by funding from the Netherlands Earth System Science Center (NESSC) through a gravitation grant (NWO 024.002.001) from the Dutch Ministry for Education, Culture and Science to J. S. S. D. and S. S. L. L. was supported by grants of the Ministry of Science and Technology (MOST) , Taiwan ROC (10-2119-M-002-003, 104-2917-I-564-046, and 105-2119-M-002-001), National Natural Science Foundation of China (41773116), State Key Laboratory of Isotope Geochemistry, Guangzhou Institute of Geochemistry, Chinese Academy of Sciences start-up fund and 135 project (SKLaBIG-QD-16-04 and 135 PY201605). Samples of core MD01-2414 and core-top samples were generously provided by Taiwan Ocean Research Institute (TORI) and S.A. Gorbarenko, respectively. Data are available at Pangaea (doi: 10.1594/PANGAEA.890820).

References

Belt, S., Massé, G., Rowland, S. J., Poulin, M., Michel, C., & LeBlanc, B. (2007). A novel chemical fossil of palaeo sea ice: IP_{25}. *Organic Geochemistry*, *38*(1), 16–27. https://doi.org/10.1016/j.orggeochem.2006.09.013

Bosin, A., Gorbarenko, S., Xuefa, S., Liu, Y., & Zou, J. (2015). Regionalized primary paleoproduction variability in the Sea of Okhotsk during late Pleistocene and Holocene. *Journal of Asian Earth Science*, *114*, 534–540. https://doi.org/10.1016/j.jseaes.2015.07.019

Brassell, S. C., Eglinton, G., Marlowe, I. T., & Sarnthein, M. (1986). Molecular stratigraphy: A new tool for climatic assessment. *Nature*, *320*(6058), 129–133. https://doi.org/10.1038/320129a0

Broerse, A. T. C., Ziveri, P., & Honjo, S. (2000). Coccolithophore ($-CaCO_3$) flux in the sea of Okhotsk: Seasonality, settling and alteration processes. *Marine Micropaleontology*, *39*(1–4), 179–200. https://doi.org/10.1016/S0377-8398(00)00020-7

Chou, Y., Lee, T., Song, S., & Chen, K. (2011). Magnetostratigraphy of marine sediment core MD01-2414 from Okhotsk Sea and its paleoenvironmental implications. *Marine Geology*, *284*(1-4), 149–157. https://doi.org/10.1016/j.margeo.2011.03.015

De Bar, M., Dorhout, D. J. C., Hopmans, E. C., Sinninghe Damsté, J. S., & Schouten, S. (2016). Constraints on the application of long chain diol proxies in the Iberian Atlantic margin. *Organic Geochemistry*, *101*, 184–195. https://doi.org/10.1016/j.orggeochem.2016.09.005

De Jonge, C., Hopmans, E. C., Stadnitskaia, A., Rijpstra, W. I. C., Hofland, R., Tegelaar, E., & Sinninghe Damsté, J. S. (2013). Identification of novel penta- and hexamethylated branched glycerol dialkyl glycerol tetraethers in peat using HPLC–MS2, GC–MS and GC–SMB-MS. *Organic Geochemistry*, *54*, 78–82. https://doi.org/10.1016/j.orggeochem.2012.10.004

De Jonge, C., Stadnitskaia, A., Hopmans, E. C., Cherkashov, G., Fedotov, A., & Sinninghe Damsté, J. S. (2014). In situ produced branched glycerol dialkyl glycerol tetraethers in suspended particulate matter from the Yenisei River, Eastern Siberia. *Geochimica et Cosmochimica Acta*, *125*, 476–491. https://doi.org/10.1016/j.gca.2013.10.031

De la Torre, J., Walker, C. B., Ingalls, A. E., Könneke, M., & Stahl, D. A. (2008). Cultivation of a thermophilic ammonia oxidizing archaeon synthesizing crenarchaeol. *Environmental Microbiology*, *10*(3), 810–818. https://doi.org/10.1111/j.1462-2920.2007.01506.x

Gelin, F., Boogers, I., Noordeloos, A. A., Sinninghe Damsté, J. S., Riegman, R., & De Leeuw, J. W. (1997). Resistant biomacromolecules in marine microalgae of the classes Eustigmatophyceae and Chlorophyceae: Geochemical implications. *Organic Geochemistry*, *26*(11–12), 659–675. https://doi.org/10.1016/S0146-6380(97)00035-1

Gong, C., & Hollander, D. J. (1999). Evidence for differential degradation of alkenones under contrasting bottom water oxygen conditions: Implication for paleotemperature reconstruction. *Geochimica et Cosmochimica Acta*, *63*(3-4), 405–411. https://doi.org/10.1016/S0016-7037(98)00283-X

Gorbarenko, S. (1996). Stable isotope and lithologic evidence of late-glacial and Holocene oceanography of the northwestern Pacific and its marginal seas. *Quaternary Research*, *46*(03), 230–250. https://doi.org/10.1006/qres.1996.0063

Gorbarenko, S. A., Artemova, A. V., Goldberg, E. L., & Vasilenko, Y. P. (2014). The response of the Okhotsk Sea environment to the orbital-millennium global climate changes during the Last Glacial Maximum, deglaciation and Holocene. *Global and Planetary Change*, *116*, 76–90. https://doi.org/10.1016/j.gloplacha.2014.02.002

Harada, N., Ahagon, N., Sakamoto, T., Uchida, M., Ikehara, M., & Shibata, Y. (2006). Rapid fluctuation of alkenones temperature in the southwestern Okhotsk Sea during the past 120 ky. *Global and Planetary Change*, *53*(1-2), 29–46. https://doi.org/10.1016/j.gloplacha.2006.01.010

Harada, N., Ahagon, N., & Uchida, M. (2004). Northward and southward migrations of frontal zones during the past 40 kyr in the Kurushio-Oyashio transition area. *Geochemistry, Geophysics, Geosystems*, *5*, Q09004. https://doi.org/10.1029/2004GC000740

Harada, N., Katsuki, K., Nakagawa, M., Matsumoto, A., Seki, O., Addison, J., et al. (2014). Holocene sea surface temperature and sea ice extent in the Okhotsk and Bering Seas. *Progress in Oceanography*, *126*, 242–253. https://doi.org/10.1016/j.pocean.2014.04.0170079-6611

Harada, N., Sato, M., Seki, O., Timmermann, A., Moossen, H., Bendle, J., et al. (2012). Sea surface temperature changes in the Okhotsk Sea and adjacent North Pacific during the last glacial maximum and deglaciation. *Deep Sea Research, Part II*, *61-64*, 93–105. https://doi.org/10.1016/j.dsr2.2011.12.007

Ho, S. L., Mollenhauer, G., Fietz, S., Martínez-Garcia, A., Lamy, F., Rueda, G., et al. (2014). Appraisal of TEX_{86} and TEX_{86}^{L} thermometries in subpolar and polar regions. *Geochimica et Cosmochimica Acta*, *131*, 213–226. https://doi.org/10.1016/j.gca.2014.01.001

Hoefs, M. J., Versteegh, G. J., Rijpstra, W. I. C., Leeuw, J. W., & Sinninghe Damsté, J. S. (1998). Postdepositional oxic degradation of alkenones: Implications for the measurement of palaeo sea surface temperatures. *Paleoceanography*, *13*(1), 42–49. https://doi.org/10.1029/97PA02893

Hopmans, E. C., Schouten, S., & Sinninghe Damsté, J. S. (2016). The effect of improved chromatography on GDGT-based palaeoproxies. *Organic Geochemistry*, *93*, 1–6. https://doi.org/10.1016/j.orggeochem.2015.12.006

Hopmans, E. C., Weijers, J., Schefuß, E., Herfort, L., Sinninghe Damsté, J. S., & Schouten, S. (2004). A novel proxy for terrestrial organic matter in sediments based on branched and isoprenoid tetraether lipids. *Earth and Planetary Science Letters*, *224*(1-2), 107–116. https://doi.org/10.1016/j.epsl.2004.05.012

Huguet, C., Kim, J.-H., Sinninghe Damsté, J. S., & Schouten, S. (2006). Reconstruction of sea surface temperature variations in the Arabian Sea over the last 23 kyr using organic proxies (TEX_{86} and $U^{k'}_{37}$). *Paleaoceanography*, *21*, PA3003. https://doi.org/10.1029/2005PA001215

Huguet, C., Schimmelmann, A., Thunell, R., Lourens, L. J., Sinninghe Damsté, J. S., & Schouten, S. (2007). A study of the TEX_{86} paleothermometer in the water column and sediments of the Santa Barbara Basin, California. *Paleoceanography*, *22*, PA3203. https://doi.org/10.1029/2006PA001310

Iwasaki, S., Takahashi, K., Maesawa, T., Sakamoto, T., Sakai, S., & Iijima, K. (2012). Paleoceanography of the last 500 kyr in the central Okhotsk Sea based on geochemistry. *Deep Sea Research, Part II*, *61-64*, 50–62. https://doi.org/10.1016/j.dsr2.2011.03.003

Jonas, A. S., Schwark, L., & Bauersachs, T. (2017). Late Quaternary water temperature variations of the Northwest Pacific based on lipid paleothermometers TEX^{H}_{86}, $U^{k'}_{37}$ and LDI. *Deep Sea Research, Part I*, *125*, 81–93. https://doi.org/10.1016/j.dsr.2017.04.018

Katsuki, K., Khim, B.-K., Itaki, K., Okazaki, Y., Ikehara, K., Shin, Y., et al. (2010). Sea-ice distribution and atmospheric pressure patterns in southwestern Okhotsk Sea since the Last Glacial Maximum. *Global and Planetary Change*, *72*(3), 99–107. https://doi.org/10.1016/j.gloplacha.2009.12.005

Khim, B. K., Sakamoto, T., & Harada, N. (2012). Reconstruction of surface water conditions in the central region of the Okhotsk Sea during the last 180 kyrs. *Deep Sea Research Part II: Topical Studies in Oceanography*, *61-64*, 63–72. https://doi.org/10.1016/j.dsr2.2011.05.014

Kim, J.-H., Crosta, X., Michel, E., Schouten, S., Duprat, J., & Sinninghe Damsté, J. S. (2009). Impact of lateral transport on organic proxies in the Southern Ocean. *Quaternary Research*, *71*(02), 246–250. https://doi.org/10.1016/j.yqres.2008.10.005

Kim, J.-H., Schouten, S., Rodrigo-Gámiz, M., Rampen, S., Marino, G., Huguet, C., et al. (2015). Influence of deep-water derived isoprenoid tetraether lipids on the paleothermometer in the Mediterranean Sea. *Geochemica and Cosmochimica Acta*, *150*, 125–141. https://doi.org/10.1016/j.gca.2014.11.017

Kim, J.-H., van der Meer, M., Schouten, S., Helmke, P., Willmott, V., Sangiorgi, F., et al. (2010). New indices and calibrations derived from the distribution of crenarchaeol isoprenoid tetraether lipids: Implication for past sea surface temperature reconstructions. *Geochemica and Cosmochimica Acta*, *74*(16), 4639–4654. https://doi.org/10.1016/j.gca. 2010.05.027

Knies, J., Cabedo-Sanz, P., Belt, S. T., Baranwal, S., Fietz, S., & Rosell-Melé, A. (2014). The emergence of modern sea ice cover in the Arctic Ocean. *Nature Communications*, *5*(1), 5608. https://doi.org/10.1038/ncomms6608

Lattaud, J., Dorhout, D., Schulz, H., Castañeda, I. C., Schefuss, E., Sinninghe Damsté, J. S., & Schouten, S. (2017). The C_{32} alkane-1,15-diol as a proxy for late Quaternary riverine input in coastal margin. *Climate of the Past*, *13*(8), 1049–1061. https://doi.org/10.5194/cp-13-1049-2017

Lattaud, J., Kim, J.-H., De Jonge, C., Zell, C., Sinninghe Damsté, J. S., & Schouten, S. (2017). The C_{32} alkane-1,15-diol as a tracer for riverine input in coastal seas. *Geochimica et Cosmochimica Acta*, *202*, 146–158. https://doi.org/10.1016/j.gca.2016.12.030

Leinen, M., Cwienk, D., Heath, G. R., Biscaye, P. E., Kolla, V., Thiede, J., & Dauphin, J. P. (1986). Distribution of biogenic silica and quartz in recent deep-sea sediments. *Geology*, *14*, 199–203. https://doi.org/10.1130/0091-7613(1986)14%3C199:DOBSAQ%3E2.0.CO;2

Lisiecki, L., & Raymo, M. (2005). A Pliocene-Pleistocene stack of 57 globally distributed benthic $\delta^{18}O$ records. *Paleoceanography*, *20*, PA1003. https://doi.org/10.1029/2004PA001071

Liu, Y.-J., Song, S.-R., Lee, T.-Q., Lee, M.-Y., Chen, Y.-L., & Chen, H.-F. (2006). Mineralogical and geochemical changes in the sediments of the Okhotsk Sea during deglacial periods in the past 500 kys. *Global and Planetary Change*, *52*, 47–57. https://doi.org/10.1016/j.gloplacha.2006.01.007

Lo, L., Belt, S., Lattaud, J., Friedrich, T., Zeeden, C., Schouten, S., et al. (2018). Precession and atmospheric CO_2 modulated variability of sea ice in the central Okhotsk Sea since 130,000 years ago. *Earth and Planetary Science Letters*, *488*, 36–45. https://doi.org/10.1016/j.epsl.2018.02.005

Locarnini, R. A., Mishonov, A. V., Antonov, J. I., Boyer, T. P., & Garcia, H. E. (2010). *World Ocean Atlas 2009, Volume 1: Temperature. S. Levitus, (Ed.), NOAA Atlas NESDIS 68* (p. 184). Washington, DC: U.S. Government Printing Office.

Lopes dos Santos, R. A., Spooner, M. I., Barrows, T. T., De Deckker, P., Sinninghe Damsté, J. S., & Schouten, S. (2013). Comparison of organic ($\mathbf{U^{k'}_{37}}$, TEX^{H}_{86}, LDI) and faunal proxies (foraminiferal assemblages) for reconstruction of late Quaternary sea surface temperature variability from offshore southeastern Australia. *Paleoceanography*, *28*, 377–387. https://doi.org/10.1002/palo.20035

Martinez-Garcia, A., Rosell-Mele, A., McClymont, E., Gersonde, R., & Haug, G. (2010). Subpolar link to the emergence of the Modern Equatorial Pacific cold tongue. *Science*, *328*, 550–553. https://doi.org/10.1126/science.1184480

Martrat, B., Jimenez-Amat, P., Zahn, R., & Grimalt, J. (2014). Similarities and dissimilarities between the last two deglaciations and interglaciations in the North Atlantic region. *Quaternary Science Reviews*, *99*, 122–134. https://doi.org/10.1016/j.quascirev.2014.06.0163

Méjanelle, L., Sanchez-Gargallo, A., Bentaleb, I., & Grimalt, J. O. (2003). Long chain n-alkyl diols, hydroxy ketones and sterols in a marine eustigmatophyte, *Nannochloropsis gaditana*, and in Brachionus plicatilis feeding on the algae. *Organic Geochemistry*, *34*(4), 527–538. https://doi.org/10.1016/S0146-6380(02)00246-2

Mollenhauer, G., Eglinton, T., Hopmans, E., & Sinninghe Damsté, J. S. (2008). A radiocarbon-based assessment of the preservation characteristics of crenarchaeol and alkenones from continental margin sediments. *Organic Geochemistry*, *39*(8), 1039–1045. https://doi.org/10.1016/j.orggeochem.2008.02.006

Müller, P. J., Kirst, G., Ruhland, G., Storch, I. V., & Rosell-Mele, A. (1998). Calibration of the alkenone paleotemperature index $U^{K'}_{37}$ based on core-tops from the eastern South Atlantic and the global ocean (60°N–60°S). *Geochimica et Cosmochimica Acta*, *62*, 1757–1772. https://doi.org/10.1016/S0016-7037(98)00097-0

Naafs, B. D. A., Hefter, J., & Stein, R. (2012). Application of the long-chain diol index (LDI) paleothermometer to the early Pleistocene (MIS 96). *Organic Geochemistry*, *49*, 83–85. https://doi.org/10.1016/j.orggeochem.2012.05.011

Nürnberg, D., Dethleff, D., Tiedemann, R., Kaiser, A., & Gorbarenko, S. (2011). Okhotsk Sea ice coverage and Kamchatka glaciation over the last 350 ka—Evidence from ice-rafted debris and planktonic $\delta^{18}O$. *Palaeogeography, Palaeoclimatology, Palaeoecology*, *310*(3-4), 191–205. https://doi.org/10.1016/j.palaeo.2011.07.011

Plancq, J., Grossi, V., Pittet, B., Huguet, C., Rosell-Melé, A., & Mattioli, E. (2015). Multi-proxy constraints on sapropel formation during the late Pliocene of central Mediterranean (southwest Sicily). *Earth and Planetary Science Letters*, *420*, 30–44. https://doi.org/10.1016/j.epsl.2015.03.031

Prahl, F., Muehhlausen, L., & Zalhne, D. (1988). Further evaluation of long-chain alkenones as indicators of paleoceanographic conditions. *Geochemica and Cosmochimica Acta*, *52*(9), 2303–2310. https://doi.org/10.1016/0016-7037(88)90132-9

Prahl, F., & Wakeham, S. G. (1987). Calibration of unsaturation patterns in long-chain ketone compositions for palaeotemperature assessment. *Nature*, *330*(6146), 367–369. https://doi.org/10.1038/330367a0

Prahl, F. G., Sparrow, M. A., & Wolfe, G. V. (2003). Physiological impacts on alkenone paleothermometry. *Paleoceanography*, *18*(2), 1025. https://doi.org/10.1029/2002PA000803

Rampen, S., Willmott, V., Kim, J., Uliana, E., Mollenhauer, G., Schefuß, E., et al. (2012). Long chain 1,13- and 1,15-diols as a potential proxy for palaeotemperature reconstruction. *Geochimica et Cosmochimica Acta*, *84*, 204–216. https://doi.org/10.1016/j.gca.2012.01.024

Rampen, S. W., Schouten, S., & Sinninghe Damsté, J. S. (2011). Occurrence of long chain 1, 14-diols in *Apedinella radians*. *Organic Geochemistry*, *42*(5), 572–574. https://doi.org/10.1016/j.orggeochem. 2011.03.009

Rampen, S. W., Schouten, S., Wakeham, S. G., & Sinninghe Damsté, J. S. (2007). Seasonal and spatial variation in the sources and fluxes of long chain diols and mid-chain hydroxy methyl alkanoates in the Arabian Sea. *Organic Geochemistry*, *38*(2), 165–179. https://doi.org/10.1016/j.orggeochem.2006.10.008

Ritchie, J., Cwynar, L., & Spear, R. (1983). Evidence from Northwest Canada for an early Holocene Milankovitch Thermal Maximum. *Nature*, *305*(5930), 126–128. https://doi.org/10.1038/305126a0

Rodrigo-Gámiz, M., Martinez-Ruiz, F., Rampen, S. W., Schouten, S., & Sinninghe Damsté, J. S. (2014). Sea surface temperature variations in the western Mediterranean Sea over the last 20 kyr: a dual organic-proxy (Uk'37, LDI) approach. *Paleoceanography*, *29*, 87–98. https://doi.org/10.1002/2013PA002466

Rodrigo-Gámiz, M., Rampen, S. W., de Haas, H., Baas, M., Schouten, S., & Sinninghe Damsté, J. S. (2015). Constraints on the applicability of the organic temperature proxies $U^{K'}_{37}$, TEX_{86} and LDI in the subpolar region around Iceland. *Biogeosciences*, *12*(22), 6573–6590. https://doi.org/10.5194/bg-12-6573-2015

Rodrigo-Gámiz, M., Rampen, S. W., Schouten, S., & Sinninghe Damsté, J. S. (2016). The impact of oxic degradation on long chain alkyl diol distributions in Arabian Sea surface sediments. *Organic Geochemistry*, 100, 1–9. https://doi.org/10.1016/j.orggeochem.2016.07.003

Rontani, J.-F., Volkman, J. K., Prahl, F. G., & Wakeham, S. G. (2013). Biotic and abiotic degradation of alkenones and implications for $U^{K'}_{37}$ paleoproxy applications: A review. *Organic Geochemistry*, *59*, 95–113. https://doi.org/10.1016/j.orggeochem.2013.04.005

Salonen, J. S., Seppä, H., Väliranta, M., Jones, V. J., Self, A., Heikkilä, M., et al. (2011). The Holocene thermal maximum and late-Holocene cooling in the tundra of NE European Russia. *Quaternary Research*, *75*(03), 501–511. https://doi.org/10.1016/j.yqres.2011.01.007

Schouten, S., Hopmans, E. C., Schefuß, E., & Sinninghe Damsté, J. S. (2002). Distributional variations in marine crenarchaeotal membrane lipids: A new tool for reconstructing ancient sea water temperatures? *Earth and Planetary Science Letters*, *204*(1-2), 265–274. https://doi.org/10.1016/S0012-821X (02)00979-2

Seki, O., Bendle, J., Harada, N., Kobayashi, M., Sawada, K., Moossen, H., et al. (2014). Assessment and calibration of TEX_{86} paleothermometry in the Sea of Okhotsk and sub-polar North Pacific region: Implications for paleoceanography. *Progress in Oceanography*, *126*, 254–266. https://doi.org/10.1016/j.pocean.2014.04.013

Seki, O., Kawamura, K., Ikehara, M., Nakatsuka, T., & Oba, T. (2004). Variation of alkenone sea surface temperature in the Sea of Okhotsk over the last 85 kyr. *Organic Geochemistry*, *34*, 347–354. https://doi.org/10.1016/j.orggeochem.2003.10.011

Seki, O., Nakatsuka, T., Kawamura, K., Saitoh, S., & Wakatsuchi, M. (2007). Time-series sediment trap record of alkenones from the western Sea of Okhotsk. *Marine Chemistry*, *104*(3-4), 253–265. https://doi.org/10.1016/j.marchem.2006.12.002

Seki, O., Sakamoto, T., Sakai, S., Schouten, S., Hopmans, E., Sinninghe Damsté, J. S., & Pancost, R. (2009). Large changes in seasonal sea ice distribution and productivity in the Sea of Okhotsk during the deglaciations. *Geochemistry, Geophysics, Geosystems*, *10*, Q10007. https://doi.org/10.1029/2009GC002613

Shackleton, N. J., Sánchez-Goñi, M. F., Pailler, D., & Lancelot, Y. (2003). Marine isotope substage 5e and the Eemian interglacial. *Global and Planetary Change*, *36*(3), 151–155. https://doi.org/10.1016/S0921-8181(02)00181-9

Shiga, K., & Koizumi, I. (2000). Latest Quaternary oceanographic changes in the Okhotsk Sea based on diatom records. *Marine Micropaleontology*, *38*, 91–117. https://doi.org/10.1016/S0377-8398(99)00041-9

Shimada, C., & Hasegawa, S. (2001). Paleoceanographic implication of a 90,000 years long diatoms record in piston core KH94-3, LM-8 off NE Japan. *Marine Micropaleontology*, *41*(3-4), 153–166. https://doi.org/10.1016/S0377-8398(00)00059-1

Shintani, T., Yamamoto, M., & Chen, M.-T. (2011). Paleoenvironmental changes in the northern South China Sea over the past 28,000 years: A study of TEX-derived sea surface temperatures and terrestrial biomarkers. *Journal of Asian Earth Sciences*, *40*(6), 1221–1229. https://doi.org/10.1016/j.jseaes. 2010.09.013

Sikes, E., Volkman, J., Robertson, L., & Pichon, J.-J. (1997). Alkenones and alkenes in surface waters and sediments of the Southern Ocean: Implications for paleotemperature estimation in polar regions. *Geochimica et Cosmochimica Acta*, *61*(7), 1495–1505. https://doi.org/10.1016/S0016-7037(97)00017-3

Sikes, E. L., O'Leary, T., Nodder, S. D., & Volkman, J. K. (2005). Alkenone temperature records and biomarker flux at the subtropical front on the Chatham rise, SW Pacific Ocean. *Deep Sea Research Part I*, *52*(5), 721–748. https://doi.org/10.1016/j.dsr.2004.12.003

Sinninghe Damsté, J. S., Rijpstra, W. I. C., Abba, B., Muyzer, G., & Schouten, S. (2003). A diatomaceous origin for long-chain diols and mid-chain hydroxy methyl alkanoates widely occurring in Quaternary marine sediments: Indicators for high nutrient conditions. *Geochimica et Cosmochimica Acta*, *67*(7), 1339–1348. https://doi.org/10.1016/S0016-7037(02)01225-5

Smith, M., De Deckker, P., Rogers, J., Brocks, J., Hope, J., Schmidt, S., et al. (2013). Comparison of organic ($U^{K'}_{37}$, TEX^{H}_{86}, LDI) and faunal proxies (foraminiferal assemblages) for reconstruction of late Quaternary sea surface temperature variability from offshore southeastern Australia. *Organic Geochemistry*, *64*, 94–104. https://doi.org/10.1016/j.orggeochem.2013.08.015

Sorokin, Y. I., & Sorokin, P. Y. (1999). Production in the Sea of Okhotsk. *Journal of Plankton Research*, *21*(2), 201–230. https://doi.org/10.1093/plankt/21.2.201

Tierney, J. E., & Tingley, M. P. (2015). A TEX_{86} surface sediment database and extended Bayesian calibration. *Scientific Data*, *2*, 150029. https://doi.org/10.1038/sdata.2015.29

Tierney, J. E., & Tingley, M. P. (2018). BAYSPLINE: A new calibration of the alkenone paleothermometer. *Paleoceanography and Paleoclimatology*, *33*, 281–301. https://doi.org/10.1002/2017PA003201

Tsunogai, S., Ono, T., & Watanabe, S. (1992). Increase in total carbonate in the western North Pacific water and a hypothesis on the missing sink of anthropogenic carbon. *Journal of Oceanography*, *49*(3), 305–315. https://doi.org/10.1007/BF02269568

Versteegh, G. J. M., Bosch, H.-G., & De Leeuw, J. W. (1997). Potential paleoenvironmental information of C24 to C36 mid-chain diols, keto-ols and mid-chain hydroxy fatty acids; a critical review. *Organic Geochemistry*. *27*, 1–13. https://doi.org/10.1016/S0146-6380(97)00063-6

Volkman, J. K., Barrett, S. M., Dunstan, G. A., & Jeffrey, S. W. (1992). C_{30}–C_{32} alkyl diols and unsaturated alcohols in microalgae of the class Eustigmatophyceae. *Organic Geochemistry*, *18*, 31–138. https://doi.org/10.1016/0146-6380(92)90150-V

Volkman, J. K., Barett, S. M., & lackburn, S. I. (1999). Eustigmatophyte microalgae are potential sources of C_{29} sterols, C_{22}–C_{28} n-alcohols and C_{28}–C_{32} n-alkyl diols in freshwater environments. *Organic Geochemistry*, *30*, 307–318. https://doi.org/10.1016/S0146-6380(99)00009-1

Wakatsuchi, M., & Martin, S. (1991). Water circulation in the Kuril basin of the Okhotsk Sea and its relation to eddy formation. *Journal Oceanography Society Japan*, *47*(4), 152–168. https://doi.org/10.1007/BF02301064

Weijers, J. W., Schouten, S., Hopmans, E., Geenevasen, J., David, O. R. P., Coleman, J., et al. (2006). Membrane lipids of mesophilic anaerobic bacteria thriving in peats have typical archaeal traits. *Environmental Microbiology*, *8*, 648–657. https://doi.org/10.1111/j.1462-2920.2005.00941.x

Weijers, J. W. H., Panoto, E., van Bleijswijk, J., Schouten, S., Rijpstra, W. I. C., Balk, M., et al. (2009). Constraints on the biological source (s) of the orphan branched tetraether membrane lipids. *Geomicrobiology Journal*, *26*(6), 402–414. https://doi.org/10.1080/01490450902937293

Wuchter, C., Abbas, B., Coolen, M. J. L., Herfort, L., Timmers, P., Strous, M., et al. (2006). Archaeal nitrification in the ocean. *Proceeding of the National Academy of Sciences of the United States of America*, *103*(33), 12,317–12,322. https://doi.org/10.1073/pnas.0600756103

Yasuda, T., Asahara, Y., Ichikawa, R., Nakatsuka, T., Minami, H., & Nagao, S. (2014). Distribution and transport processes of lithogenic material from the Amur River revealed by the Sr and Nd isotope ratios of sediments from the Sea of Okhotsk. *Progress in Oceanography*, *126*, 155–167. https://doi.org/10.1016/j.pocean.2014.04.015